RESEARCH ARTICLE

Object color knowledge representation occurs in the macaque brain despite the absence of a developed language system

Minghui Zhao[1,2], Yumeng Xin[1,2], Haoyun Deng[1,2], Zhentao Zuo[1,2,3], Xiaoying Wang[4,5]*, Yanchao Bi[4,5,6,7]*, Ning Liu[1,2]*

1 State Key Laboratory of Brain and Cognitive Science, Institute of Biophysics, Chinese Academy of Sciences,

complex tools and language [1,2]. How semantic memory (i.e., general knowledge) through life experience. Upon their arrival at the laboratory, their diet included selected fruits and vegetables with 3 diagnostic colors (Red: strawberry, watermelon; Green: cabbage, kiwi; Yellow: banana, corn). The 3 fMRI experiments probing color perception and object color knowledge included the following (Fig 1): (1) Chromatic and achromatic grating viewing (Exp 1): Macaques viewed luminance-matched chromatic (i.e., red, green, yellow) and achromatic (i.e., 25%, 50%, 75% luminance contrast) gratings, the contrast of which facilitated color patch localization; (2) grayscale object viewing (Exp 2): Macaques viewed grayscale photos of fruits and vegetables with 3 diagnostic colors (Red: strawberry, watermelon slice; Green: cabbage, kiwi slice; Yellow: banana, corn), and we tested whether brain responses to grayscale images could accurately encode objects' typical colors (i.e., reflecting memory representation); (3) true- and false-colored object viewing (Exp 3): Macaques viewed photos of correctly colored objects (i.e., red strawberry, red watermelon slice, green cabbage, green kiwi slice) and their color-swapped false counterparts (i.e., red-colored cabbage and kiwi slice; green-colored strawberry and watermelon slice), and the true/false color univariate differentiation and multivariate decoding accuracy from brain responses were examined (i.e., testing if a region could distinguish visual stimuli that correspond to real natural objects from those that do not). To avoid interference between experiments caused by the potential learning effect, we conducted the experiments in the following order: Exp 2, Exp 1, and Exp 3. Furthermore, we conducted a free-viewing visual paired comparison (VPC) task to investigate subjects' visual preference for true- and false-colored object stimuli used in Exp 3 (see S1 Text and S1A Fig).

Color patches localization

We first localized color patches along the ventral visual pathway by contrasting chromatic and achromatic gratings (Fig 1B, Exp 1). Following the previous procedure used for color patch identification [37,38], the effect of luminance was controlled by referencing the activation in MT, which is specialized to process moving stimuli and responds less strongly to moving chromatic gratings if the foreground and background within the chromatic gratings are equiluminant. We identified the chromatic grating that induced the weakest activation in MT for each monkey, as well as the corresponding achromatic grating that evoked comparable activation with the selected chromatic grating in V1. We then contrasted the activation of the selected chromatic grating and the corresponding achromatic grating, and located a series of color

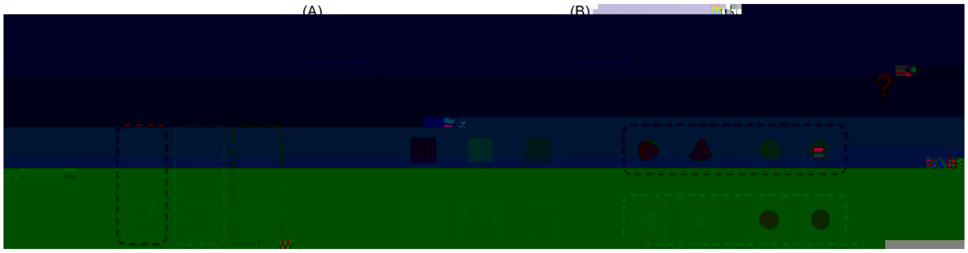

Fig 1. Experimental procedures. Three experiments were conducted and combined to investigate the neural basis for object color and related integrative object knowledge. (A) Examples of stimuli in the grayscale object viewing experiment (Exp 2): 6 types of color-diagnostic grayscale objects from 3 color categories (Red: strawberry, watermelon; Green: cabbage, kiwi; Yellow: banana, corn). (B) Examples of stimuli in the chromatic and achromatic grating viewing experiment (Exp 1): 3 equiluminant chromatic gratings (i.e., red, green, and yellow) and 3 achromatic gratings with 25%, 50%, and 75% luminance contrast that had equal mean luminance with chromatic gratings. (C) Examples of stimuli used in the true- and false-colored objects viewing experiment (Exp 3). Only red and green color categories (Red: strawberry, watermelon; Green: cabbage, kiwi) and their color-swapped false items were included in Exp 3. Three fMRI experiments were performed in the order of Exp 2, Exp 1, and Exp 3 to avoid interference between experiments caused by learning. fMRI, functional magnetic resonance imaging.

https://doi.org/10.1371/journal.pbio.3002863.g001

patches (chromatic > achromatic) in all 3 animals along the ventral visual pathway, including the color patches around V4d (V4d_c), V4v (V4v_c), TEO (TEO_c), TEpd (TEpd_c), TEad (TEad_c), TEav (TEav_c), and the boundary between areas TEa and IPa (TEa_c) (Fig 2A). Note that, to signify the locations of the color patches, we named the color patches based on their anatomical locations by appending ª_cº at the end of the brain regions where the color bias clusters were located. Please refer to S1 Table for the correspondence between the names in the present study and the corresponding names in previous studies [36,37]. Region of interest (ROI) analyses contrasting the activation of the unselected chromatic and achromatic gratings confirmed the color sensitivity in these color patches [see S2A Fig for the group generalized linear mixed model (GLMM) results with false discovery rate (FDR) correction (aka q-value); V4d_c: $F_{(1,156)} = 164.141$, $q < 0.001$, Cohen's $d = 2.052$; V4v_c: $F_{(1,155)} = 155.161$, $q < 0.001$, Cohen's $d = 2.001$; TEO_c: $F_{(1,156)} = 143.046$, $q < 0.001$, Cohen's $d = 1.915$; TEpd_c: $F_{(1,156)} = 81.590$, $q < 0.001$, Cohen's $d = 1.446$; TEad_c: $F_{(1,156)} = 61.739$, $q < 0.001$, Cohen's $d = 1.258$; TEav_c: $F_{(1,156)} = 6.603$, $q = 0.011$, Cohen's $d = 0.412$; TEa_c: $F_{(1,156)} = 9.556$, $q = 0.002$, Cohen's $d = 0.495$; two-tailed]. All of these color patches could successfully discriminate the 3 colors in the multivoxel pattern analysis (MVPA) [S2B Fig; V4d_c: $F_{(1,156)} = 205.489$, $q < 0.001$; V4v_c: $F_{(1,156)} = 103.752$, $q < 0.001$; TEO_c: $F_{(1,156)} = 209.230$, $q < 0.001$; TEpd_c: $F_{(1,156)} = 63.425$, $q < 0.001$; TEad_c: $F_{(1,156)} = 10.894$, $q < 0.001$; TEav_c: $F_{(1,156)} = 8.245$, $q = 0.002$; TEa_c: $F_{(1,156)} = 43.701$, $q < 0.001$; one-tailed; see the results of each monkey in S3 Fig].

Object color memory representation in the color patches

Classification of grayscale objects with different memory colors. We compared averaged responses to 3 categories of grayscale objects. No significant differences were found in any of the defined color patches (S4A Fig). To investigate whether color patches can encode object color knowledge in the absence of color inputs, we started by examining whether the grayscale objects with different memory colors (e.g., strawberry±kiwi) would elicit distinct response patterns, whereas those with the same memory color (e.g., strawberry±watermelon) would evoke similar response patterns in color patches.

Firstly, we trained a linear discriminant analysis (LDA) classifier [39] with a half set of the color-diagnostic objects (e.g., strawberry, cabbage, and banana) and tested it on the other half set of objects (e.g., watermelon slice, kiwi slice, and corn). As shown in S5A Fig, response patterns in color patches V4d_c, V4v_c, TEO_c, TEad_c, and TEa_c could successfully distinguish 3 categories of grayscale objects with different memory colors.

Note that previous studies have reported that color patches can also represent shape information to some extent [36]. Therefore, the above-mentioned findings in color patches may be driven by memory colors and/or shape information. To ensure the exclusion of confounding effects related to object shape, we excluded objects with yellow memory

Fig 2. Representations of object color memory in the color patches. (A) Color patches (chromatic versus achromatic grating) from Exp 1 are shown on lateral views of the template inflated surface. Note that relatively higher thresholds ($p < 0.01$ for M1, $p < 0.001$ for M2, and $p < 10^{-6}$ for M3) were applied to depict the locations of color patches without confluent activation. Red solid lines indicate that color patches ($p < 0.05$ uncorrected) could not be presented at the thresholds set for A. For M1 and M2, the achromatic grating was adjusted to the next lower level (i.e., from 50% to 25%) to localize the color patches with weak color bias in the right hemisphere [i.e., TEpd_c (CLc), TEav_c (AVc), and TEa_c (AFc) in M1, and TEad_c (ALc) in M2] at a threshold of $p < 0.05$ (uncorrected). These color patches are marked with solid white lines. (B, C) The illustration and results of classification of grayscale objects with red and green memory colors: training the classifier to distinguish a half set of the red and green color-diagnostic grayscale objects and testing on the other half. Successful memory color decoding was found in V4d_c, TEO_c, and TEad_c. (D, E) The illustration and results of memory color decoding based on chromatic gratings training: training the classifier to distinguish among 3 chromatic gratings on Exp 1 and then testing on 3 categories of grayscale objects in Exp 2. Successful memory color decoding was found in V4d_c, V4v_c, TEO_c, TEpd_c, TEad_c, and TEa_c. (F, G) The illustration and results of true-false color decoding: training on true- and false-colored objects in N-1 runs and testing on the left-out run. Significant decoding of true-false color was done only in TEO_c and TEpd_c. Bars display mean values +/− SEM. Black asterisks indicate a significant difference from the chance level (0.333 in E, 0.5 in C, and G, indicated by the dashed lines); *q < 0.05, **q < 0.01, ***q < 0.001. The data underlying this figure are available in S1 Data and https://zenodo.org/records/13739051.

https://doi.org/10.1371/journal.pbio.3002863.g002

q = 0.993; TEa_c: $F_{(1,176)} = 2.464$, q = 0.102; one-tailed]. At the individual level, significant results were found in V4d_c and TEO_c for all 3 subjects (see S7A±S7C Fig for the results of each monkey). Whole-brain searchlight results also showed that areas around the posterior color patches could successfully discriminate between objects based on their memory colors in all 3 subjects (see S7D±S7F Fig for the results of individual monkeys).

To further exclude the potential shape confound on memory color decoding, we examined the classification results for cases where shape could not help the memory color classification (for details, see S5B Fig, as marked with red frames). As shown in S5C Fig, even in this more rigorous analysis, we again observed successful differentiation between grayscale objects with different memory colors in V4d_c, TEO_c, and TEad_c [V4d_c: $F_{(1,176)} = 116.955$, q < 0.001; V4v_c: $F_{(1,176)} = 1.124$, q = 0.203; TEO_c: $F_{(1,176)} = 11.836$, q = 0.001; TEpd_c: $F_{(1,176)} = 2.725$, q = 0.088; TEad_c: $F_{(1,176)} = 7.728$, q = 0.007; TEav_c: $F_{(1,176)} = 4.007$, q = 0.977; TEa_c: $F_{(1,176)} = 0.473$, q = 0.287; one-tailed].

Decoding memory colors of grayscale objects based on responses to chromatic gratings. To more directly examine whether the object color knowledge representation aligns with actual color perceptual experience and to further eliminate the shape confound, we trained an LDA classifier with the brain activity patterns elicited by the chromatic gratings (i.e., red, green, yellow) in the chromatic and achromatic grating viewing experiment and tested it on the activity patterns evoked by the grayscale objects with different memory colors in the grayscale object viewing experiment (Red: strawberry, watermelon slice; Green: cabbage, kiwi slice; Yellow: banana, corn; Fig 2D). Since the classifier was specifically trained to discriminate among chromatic gratings with only differences in color but not shape or other information, this approach has been shown to effectively address concerns about potential confounds and was widely used in many previous human studies [10,40,41]. Classification accuracies across 3 monkeys in the V4d_c, V4v_c, TEO_c, TEpd_c, TEad_c, and TEa_c were significantly higher than the chance level (0.333) [Fig 2E; V4d_c: $F_{(1,176)} = 24.816$, $q < 0.001$; V4v_c: $F_{(1,176)} = 65.443$, $q < 0.001$; TEO_c: $F_{(1,176)} = 27.569$, $q < 0.001$; TEpd_c: $F_{(1,176)} = 3.485$, $q = 0.045$; TEad_c: $F_{(1,176)} = 3.176$, $q = 0.045$; TEav_c: $F_{(1,176)} = 2.157$, $q = 0.072$; TEa_c: $F_{(1,176)} = 12.256$, $q < 0.001$; one-tailed]. Especially, in V4v_c and TEO_c, we consistently observed significant or marginally significant results across all 3 subjects (see the results of each monkey in S8A±S8C Fig). Whole-brain searchlight analyses in all 3 monkeys also confirmed that areas whose neural patterns successfully translate between chromatic gratings and grayscale objects with corresponding memory colors were mainly distributed in the color patches and their surrounding regions (S8D±S8F Fig).

As shown in S7D±S7F and S8D±S8F Figs, the searchlight results did reveal clusters in the primary visual cortex (V1) that could significantly encode memory color. However, it is worth noting that the location of these clusters was not consistent across 3 monkeys and across the memory color decoding approaches. Further analyses based on the defined ROI in V1 (the top 50 voxels with the strongest averaged responses to 6 grayscale objects) showed that V1 could not classify grayscale objects with red and green memory colors [S9A Fig: $F_{(1,176)} = 0.031$, $p = 0.431$; one-tailed] but could successfully encode memory color when trained on chromatic gratings [S9B Fig: $F_{(1,176)} = 3.484$, $p = 0.032$; one-tailed].

Differentiation between true- and false-colored objects. We further corroborated the findings of object color memory representation in the color patches with a true- and false-colored object viewing experiment (e.g., red strawberry versus green strawberry, Fig 1C, Exp 3). The false-colored object images were created by swapping the colors among the true-colored object items. Thus, the true- and false-colored objects were perfectly matched in terms of shapes and colors. The only difference between these 2 conditions was whether the combination of color and shape information matched the long-term memory representations of these objects obtained from daily experience. We first compared the activation strengths to true- and false-colored objects. Among the color patches, no regions exhibited significant differences in activation strength between these 2 conditions (S10 Fig; see S2 Table for statistical results of each region). MVPA decoding between true- and false-colored objects revealed that the activation patterns in color patches TEO_c and TEpd_c could differentiate between the 2 types of object images [Fig 2F and 2G; V4d_c: $F_{(1,128)} = 0.748$, $q = 0.272$; V4v_c: $F_{(1,128)} = 4.176$, $q = 0.050$; TEO_c: $F_{(1,128)} = 34.153$, $q < 0.001$; TEpd_c: $F_{(1,128)} = 7.123$, $q = 0.015$; TEad_c: $F_{(1,128)} = 1.907$, $q = 0.149$; TEav_c: $F_{(1,128)} = 5.202$, $q = 0.988$; TEa_c: $F_{(1,128)} = 0.101$, $q = 0.438$; one-tailed]. The classification accuracy for all 3 monkeys surpassed the chance level, with significant results found in 2 of the 3 subjects (see S11A±S11C Fig for the results of individual monkeys). Similar results were obtained in the whole-brain searchlight analyses: significant true-false encoding regions were distributed mainly in the dorsal inferotemporal (IT) cortex, particularly surrounding the TEO_c and TEpd_c (S11D±S11F Fig).

Taken together, we consistently observed the representation of object color memory in the posterior color perceptual regions (especially in TEO_c) across multiple experiments and decoding analyses.

Note that there was some inter-hemispheric and inter-animal variability in the localization of defined color patches, as discussed in the previous study [37]. To ensure greater consistency in the locations of the color patches across different monkeys, we also conducted analyses on color patches defined on the averaged activation map across 3 subjects (see S2 Text and S12A Fig). Although the group-defined ROIs might not correspond to the most color biased voxels for each individual subject, we again observed similar results, especially for the color patch around TEOon

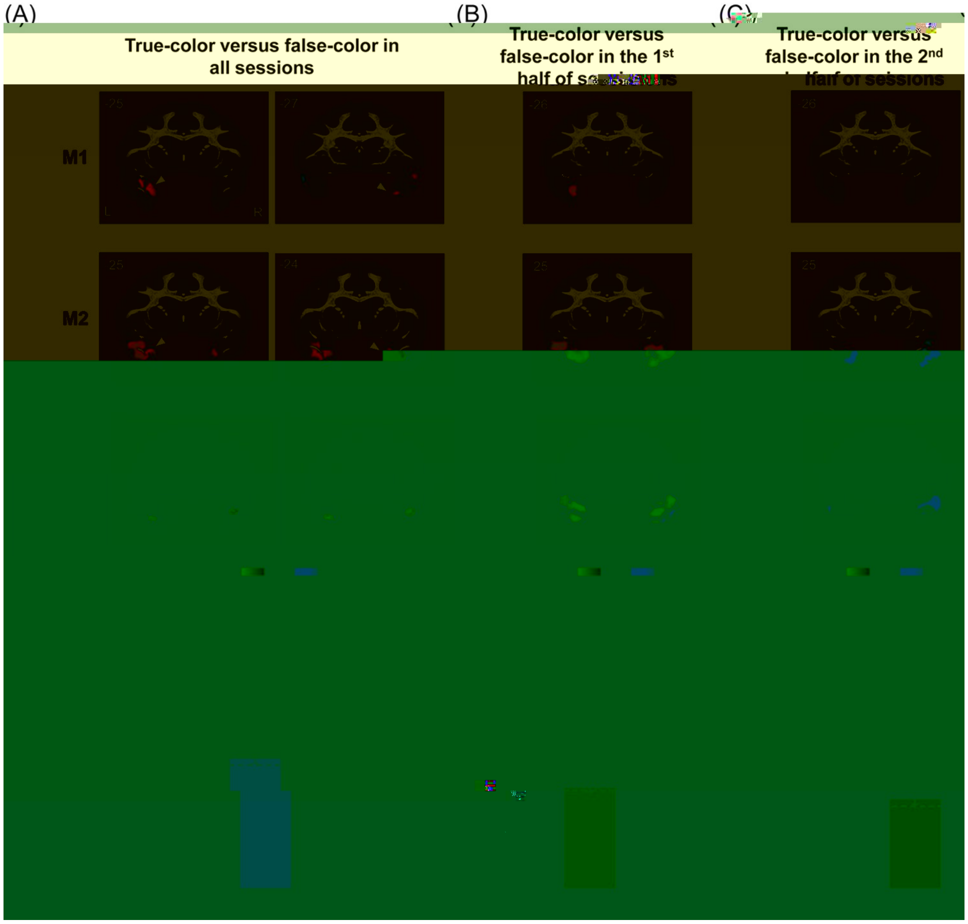

Fig 3. Representations of object color memory in TP. (A±C) The true-color versus false-color in all sessions (A), the first part of sessions (B), and the second part of sessions (C) in TP are shown in the coronal slices for each of the 3 subjects (M1 to M3) at $p < 0.05$, respectively. Each slice's anterior/posterior position is indicated on the top left corner (mm relative to the interaural canal). (D) True-false color decoding accuracy when combining all the sessions in TP. (E) Classification of grayscale objects with red and green memory colors in TP. (F) Memory color decoding accuracy based on chromatic gratings training in TP. Bars display mean values +/− SEM. The dashed lines indicate chance levels (0.5 in D and E, 0.333 in F). The data underlying this figure are available in S1 Data and https://zenodo.org/records/13739051. TP, temporal pole.

https://doi.org/10.1371/journal.pbio.3002863.g003

tailed; see S18A±S18C Fig for the results of individual monkeys] or when the first and second halves were analyzed separately [S19A Fig; first half (all sessions): F $_{(1,66)}$ = 0.020, q = 0.556; second half (all sessions): F $_{(1,60)}$ = 0.012, q = 0.543; one-tailed; see S18D±S18F Fig for the results of individual monkeys].

We conducted the same decoding analyses in PR as those performed in TP and did not find significant results (S18 and S19 Figs).

To check whether the above-mentioned learning effect also existed in the color patches, we conducted the same analyses in the color patches. None of these regions showed significant modulation by the short-term familiarization of false-colored objects in either the univariate contrast analyses (S20A Fig and S4 Table) or the MVPA [S20B Fig; V4d_c: F $_{(1,63)}$ = 1.634, q = 0.401; V4v_c: F $_{(1,63)}$ = 0.009, q = 0.925; TEO_c: F $_{(1,63)}$ = 2.343, q = 0.401; TEpd_c: F $_{(1,63)}$ = 1.777, q = 0.401; TEad_c: F $_{(1,63)}$ = 0.635, q = 0.600; TEav_c: F $_{(1,63)}$ = 1.476, q = 0.401; TEa_c: F $_{(1,63)}$ = –0.196, q = 0.770; two-tailed; see S21 Fig for the results of individual monkeys]. Note that the whole-brain analysis revealed that only TP showed a significant interaction effect between Period (first half versus second half of sessions) and true-false at the group level (S16C Fig).

Lack of specific coding of object memory color in TP. Unsurprisingly, there were no significant differences in responses to 3 categories of grayscale objects in TP (S4C Fig). We did not observe successful encoding of object memory color of grayscale objects in TP in the whole-brain searchlight results (see S7D±S7F and S8D±S8F Figs). To conservatively test whether TP also encoded the specific object color information, we examined memory color encoding of grayscale objects in the defined ROI in TP. Still, the object color information could not be significantly readout (classification of grayscale objects with red and green memory colors: see Fig 3E for the averaged results across 3 monkeys [$F_{(1,176)} = 0.401$, q = 0.527; one-tailed], see S22A Fig for the results of individual monkeys; memory color decoding based on chromatic gratings training: see Fig 3F for the averaged results across three monkeys [$F_{(1,176)} = 1.710$, q = 0.161; one-tailed], see S22B Fig for the results of individual monkeys). These results suggested that color information represented in TP was no longer specifically coded as a separate object feature.

Again, no significant results were found in PR in the same decoding analyses as those performed in TP (S22 Fig).

Differences in behavioral responses to true- and false-colored object images

To direct examine the existence of object color knowledge in the tested animals in the present study, we conducted one behavioral experiment. Two subjects (M2 and M3 but not M1 due to health concerns) were trained to perform a VPC task [48±50], in which a true-colored object image from the fMRI experiments was paired with the corresponding false-colored image (S1A Fig). Specifically, we tested 2 indicators: the proportion of fixation time and the proportion of first fixation [51]. The results from both indicators showed that monkeys had a stronger preference for true-colored stimuli than false-colored ones [S1B and S1C Fig; the proportion of fixation time: $F_{(1,84)} = 28.607$, $p < 0.001$, Cohen's d = 1.167; the proportion of first fixation: $F_{(1,84)} = 33.688$, $p < 0.001$, Cohen's d = 1.267; two-tailed], which indicated that monkeys are behaviorally capable of systematically distinguishing between true and false-colored stimuli, confirming the presence of object color knowledge.

Discussion

We aimed to discover how the macaque brain stores general information about the world, testing specifically the color knowledge of objects they are familiar with. The tested macaques showed a visual preference for true-colored objects, providing direct positive behavioral evidence of object color memory in macaques. Across multiple fMRI analyses, we found indications of object color knowledge representation in the color patches. Brain activity patterns in color patches, especially TEO_c, could classify grayscale object images based on their memory colors, with their activation patterns being transferrable among grayscale objects within the same diagnostic color category (e.g., grayscale images of watermelon Ð grayscale images of strawberry). Notably, activity patterns of these color patches could translate between chromatic grating viewing and grayscale object viewing (e.g., red grating Ð grayscale images of strawberry), such that classifiers trained by viewing chromatic gratings could successfully classify grayscale object images according to their diagnostic colors. Furthermore, the activity patterns in TEO_c were able to distinguish between true- and false-colored fruits and vegetables (e.g., green kiwi versus red kiwi). We also revealed that TP exhibited different patterns of color memory representation from color patches: it showed stronger responses to true- than false-colored objects; its preference for true-colored objects was diminished in the second half of

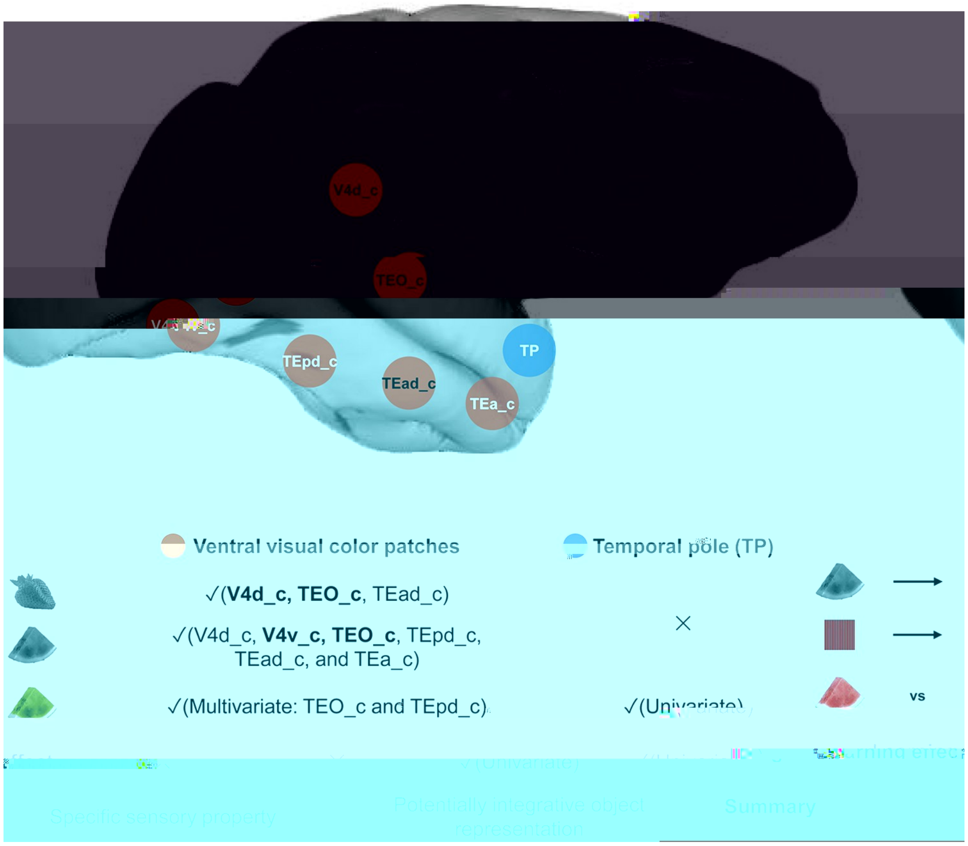

Fig 4. A schematic view of the distributed object knowledge representation in the macaque brain. Red nodes: visual color patches that could encode the typical colors of fruits and vegetables presented as grayscale pictures. Red nodes with black characters: color patches (V4d_c, TEO_c, and TEad_c), where brain activity patterns could be transferrable among grayscale objects within the same diagnostic color category. The brain regions highlighted in bold in the table indicate areas where significant or marginally significant results were consistently observed across all 3 tested monkeys. Additionally, TEO_c could encode true-false color as well, showing stable object color memory representation across 3 analyses. Blue nodes, TP, might store integrative object shape-color information that is abstracted away from specific sensory properties, which showed stronger responses to true- than false-colored objects and could not decode memory colors of grayscale objects. Only TP but not the above-mentioned color patches showed a short-term learning effect on false-colored objects. TP, temporal pole.

https://doi.org/10.1371/journal.pbio.3002863.g004

experimental sessions, indicating its sensitivity to short-term learning; however, it could not encode memory colors of grayscale object images (Fig 4).

The most novel finding of our study is the shared neural representation for chromatic grating perception and object color knowledge in the macaque brain. Our chromatic and achromatic grating viewing experiment identified color patches that responded more strongly to chromatic gratings than achromatic gratings, consistent with the literature before in macaques [37]. In addition, we found that these color patches were capable of distinguishing among red, green, and yellow. Furthermore, we demonstrated that color patches in V4d_c, TEO_c, and TEad_c could encode grayscale strawberries in red and grayscale kiwis in green, i.e., representing the color knowledge based on past perceptual experiences, just like the human brain does [11,41]. Such object color knowledge representation could not solely be attributable to shape confound: (1) brain activities to grayscale images of objects could be classified based on color beyond potential shape similarity; and (2) most compellingly, classifiers trained by chromatic grating viewing where shape information was fully uninformative could successfully decode grayscale objects based on their experienced color. Note that there is one possibility that shape information could still potentially contribute to the decoding of grayscale objects with different memory colors if there is a certain association between color and shape prevalently present in the macaques. Such a possibility has seldom been investigated in macaques at least to our knowledge (but see [52] and [36] for the possible association between face and warm hue]. In human studies, certain color-shape associations have been proposed (e.g., red-square, yellow-triangle, blue-circle) but with messily inconsistent empirical results [53,54]. Given the lack of evidence for specific color-shape associations in macaques and the fact that the proposed (but not proven) color-shape association in humans could only interfere with our memory color decoding, our current findings indicate that, without actual color inputs, the macaque brain can fill in the colors of a grayscale object based on past color perceptual experiences, a format of ªsemantic memoryº in monkeys.

While some color patches (i.e., V4d_c, TEO_c, and TEad_c) showed robust evidence for object color knowledge across multiple memory color decoding analyses, some showed variations across different analyses. Specifically, color patches in V4v_c, TEpd_c, and TEa_c showed significant results in the cross-decoding analyses between chromatic gratings and grayscale object images, but not in the cross-decoding analyses between different grayscale images. This might be because the latter analyses were performed by split-half analyses with half of the item samples in the former ones and/or because in the latter ones the classifier also picked up non-color information in the object images, potentially impacting the classifier's performance. In addition, in Exp 3, only a limited number of color patches displayed discriminability between true and false conditions based on their activation patterns. This finding could potentially be attributed to the impact of the processing of visual perceptual information, which was intentionally perfectly matched between the true- and false-colored conditions in our study, in some of the color patches. Previous magnetoencephalography (MEG) experiments in humans have shown the interplay between the processing of incoming color information and stored object knowledge [55]. Moreover, the variable patterns of decoding results between Exp 2 and Exp 3 in some color patches (e.g., TEad_c and TEpd_c) could potentially be explained by the visual color processing characteristics in each region [36]. The current experiments were not optimally designed to test such possibilities. Future research, such as studies using methods with better time resolution like electrophysiological recording, may offer valuable insights into the relationship between visual perception and memory representation in the color patches.

We also investigated the memory color encoding in V1 and found that V1 could successfully differentiate memory colors based on chromatic grating training but not when trained on grayscale objects. Note that in previous human studies, memory color representation in V1 has been inconsistently reported [10,11,41].

Previous studies in monkeys have observed backward signal transportation from ATL (e.g., PR) to TE during the visual pair-association task [56] and revealed that the laminar-specific top-down regulation from PR to TE is coupled with a successful recall of visual associates from memory [57], suggesting the engagement of the visual cortex in visual memory retrieval. However, the precise role of the visual cortex is not clear. Our finding clearly revealed the storage of object color memory in color patches. Could it be possible that what we observed in color patches is only a byproduct, a copy transported from object color memory stored elsewhere? A set of empirical observations argues against this possibility. Firstly, whole-brain searchlight analyses in the current study showed that the color knowledge decoding results for grayscale images were mainly distributed in the color patches, with effects in other brain regions (e.g., the ATL) less apparent. Secondly, human cases with color knowledge specific deficits have been related to having lesions encompassing the homologous territories of color patches in monkeys [13,14], hinting at their potentially necessary role in color knowledge representation, although the contribution of lesions beyond these regions could not be excluded. Thus, the most parsimonious explanation for our findings is that the sensory-experience-derived neural representation for knowledge constitutes a conservative mechanism for encoding object color memory.

In TP, our finding about stronger responses to object images with familiar color-shape combinations largely resonates with previous macaque findings contrasting familiar versus unfamiliar faces [33]. In addition, our results found that TP exhibited a short-term learning effect, consistent with the conventional finding that the ATL is critical in signaling object familiarity, with its neural responses modulated by repeated stimulus exposure [44±47]. The convergence of the sensitivity to familiar faces and to general shape-color combination knowledge about objects is illuminating. Note that, as shown in S10 and S20 Figs, none of the color patches showed differences between true- and false-colored objects or the short-term learning effect. To scrutinize the possibility that the univariate results in TP may be an emotional effect of familiarity originating from elsewhere in the brain, we conducted analyses in the amygdala, a crucial region involved in emotion processing and directly connected with TP [58,59]. Our results revealed no significant main effect of True-False or interaction effect between Period and True-False in the amygdala (S23 Fig). To further assess whether regions other than the color patches and amygdala showed similar univariate results to those found in TP, we conducted the whole-brain analysis. Though several brain regions showed differences in activation strengths, only TP showed a significant interaction effect between Period (first half versus second half of sessions) and True-False at the group level (S16C Fig). Therefore, it is unlikely that the univariate results observed in TP could be attributed to an emotional response originating from another brain region, such as IT and the amygdala.

In addition to the univariate results, TP also exhibited other different patterns of color memory representation from color patches: without representing specific color attributes, as evidenced by the failure to encode typical colors of grayscale objects. In previous human literature, the ATL was traditionally considered as the site for more integrative semantic memory representations abstracted from specific perceptual features ([7,18,20,26]; but see [60] and [61] for evidence for object color memory representation in dorsal ATL). For example, Coutanche and Thompson-Schill [20] showed that the ATL encodes familiar object identities without further sensitivity to specific object shapes or color properties. Our study revealed the potential encoding of object identity of true-colored stimuli in TP (S24 Fig). Our findings are in accord with the possibility that TP may act as an integration area binding together separate features in monkeys, similar to what has been proposed in human ATL. Note that we did not observe clear evidence in PR. The relatively low signal in PR due to its location could potentially account for these findings. In the previous monkey fMRI study that located familiar face regions in PR [33], a particular device was employed to enhance the signal-to-noise ratio (SNR), which may be necessary to reveal effects in PR. More generally, employing rigorous methodologies and carefully controlling for potential confounding factors, future research may provide more detailed insights into the functional role of the ATL (e.g., TP) in monkeys in relation to potential homologous regions in humans.

We observed an intriguing pattern of empirical results in the true- and false-colored objects viewing experiment: the univariate contrast analysis result did not go along with the multivariate pattern analysis result. Specifically, TP showed univariate activation differences between true- and false- conditions but could not differentiate between them based on their activation patterns. Conversely, some of the color perceptual patches (especially posterior and middle ones) exhibited an opposite functional pattern, discriminating the true versus false conditions only in their spatial activation patterns but not in their mean activation strengths. For TP, it is possible that the multivariate pattern coded the specific identity of a unique concept [19,62], whereas the general conceptual familiarity was only reflected in the neuronal activation amplitude. Indeed, we observed a high probability of encoding object identity in TP. For color patches, the lack of differentiation in activation strengths between true and false conditions might be due to the perceptual dominance of these regions, as our stimuli were well-matched in their sensory input (e.g., color and shape), whereas the memory-based difference was mainly coded in fine-grained multivariate activation patterns.

There has been limited previous evidence regarding object color knowledge in macaques, with only one study indicating that monkeys could exploit color information for categorization [63]. In this study, a behavioral study demonstrated that monkeys could ignore changes in object shape and generalize from one edible object to another based on color in conjunction with other substance properties. This finding indirectly suggested that macaques may have experiential knowledge of colors. In the present study, we conducted a behavioral experiment to measure whether these animals have developed memory colors for the stimuli we used. Our results showed that all the tested macaques showed a visual preference for true-colored objects, providing direct positive behavioral evidence of object color memory in macaques. Furthermore, our experiments directly reveal that the macaque brain can classify objects based on memory color in the absence of color visual input.

Together, these results paint a picture of distributed object knowledge representation in the macaque brain, with clear evidence about object color memory representations shared with perception in the color patches, and potentially integrative representations in the TP region of ATL. Establishing such neural representations of general world knowledge in macaque has important implications for interpreting human brain data. In humans, language and knowledge representations are notoriously difficult to tease apart [6,22±25]. In fact, congenitally blind individuals, who cannot acquire object color knowledge from sensory experiences, can nonetheless acquire similar semantic structures through the dorsal ATL (dATL) [60,61,64]. Such findings lead to the proposal of a dual-form of knowledge representation in the human brain, including both language-derived and sensory-derived knowledge representations [6]. Since the sensory-experience-independent dATL is intrinsically functionally connected with the visual-experience-derived color knowledge representation in the ventral temporal cortex, potential interactions between these 2 forms of knowledge representations could not be fully excluded in humans. The macaque data critically showed that the knowledge across color patches in our results may be attributed to their eccentricity and the resultant color selectivity. To investigate this possibility, we calculated the color selectivity for the defined color patches (see S3 Text). Our results did not show a clear relationship between the encoding ability for memory color and color selectivity (see S25 Fig). Due to technical and animal health reasons, we were not able to define a retinotopic map for each monkey here. To gain a deeper understanding, future studies could consider acquiring the retinotopic map for each monkey and conducting more precise analyses. Furthermore, the inclusion of an experimental group with visual experience and a control group without relevant experience might be more interesting and more thorough to look at the neural mechanism underlying object memory, especially helpful to provide a more comprehensive understanding of the knowledge-building process. Future studies focusing on the development of memory for object color in juvenile monkeys may provide a more comprehensive understanding of the development of object knowledge.

To conclude, we depicted how the macaque brain stores color knowledge about objects in the world: object color knowledge is stored based on visual perceptual neural activities. These findings indicate that the sensory-derived knowledge representation previously observed in the human brain is conservative and not the results of language, and thus open a new avenue for studying various aspects of semantic memory neural mechanisms with nonhuman primate models.

Methods

Subjects and general procedures

Three male rhesus monkeys (M1-M3; *Macaca mulatta*; 9 to 10 y old; 7.5 to 10 kg) were used. They were acquired from the same primate breeding facility, where they had social group histories as well as group-housing experiences until their transfer to the Institute of Biophysics (IBP), Chinese Academy of Sciences (CAS) at the age of approximately 4 years. After that, they were individually caged with auditory and visual contact with other conspecifics in the same colony room, which accommodates about 10 rhesus monkeys. All animals used in this study had been housed at IBP for 4 to 6 years before this experiment. All experimental procedures complied with the US National Institutes of Health Guide for the Care and Use of Laboratory Animals and were approved by the Institutional Animal Care and Use Committee of IBP (IBP-NHP-003). Each monkey was surgically implanted with a magnetic resonance (MR)-compatible head post under sterile conditions, using isoflurane anesthesia. After recovery, subjects were trained to sit in a plastic restraint chair and fixate on a central target for long durations with their heads fixed, facing a screen on which visual stimuli were presented [68,69].

Brain activity measurements

Functional and anatomical MRI scanning was carried out in the Beijing MRI Center for Brain Research (BMCBR). Before each scanning session, an exogenous contrast agent [monocrystalline iron oxide nanocolloid (MION)] was injected into the femoral or external saphenous vein (8 mg/kg) to increase the contrast/noise ratio and to optimize the localization of fMRI signals [70]. Imaging data were collected in a 3T Siemens Prisma MRI scanner with a surface coil array (8 elements). Forty-eight 1.5-mm coronal slices (no gap) were acquired using single-shot interleaved gradient-recalled echo planar imaging. Imaging parameters were as follows: voxel size: 1.5 mm isotropic, field of view: 129 × 129 mm; matrix size: 86 × 86; echo time (TE): 17 ms; repetition time (TR): 2.5 s; flip angle: 90Ê. A low-resolution T2 anatomical scan was also acquired in each session to serve as an anatomical reference (0.625 mm × 0.625 mm × 1.5mm; TE: 101 ms; TR: 11.2 s; flip angle: 126Ê). To facilitate the alignment to the template, we also acquired high-resolution T1-weighted whole-brain anatomical scans in separate sessions. Imaging parameters were as follows: voxel size = 0.5 mm isotropic, TE = 2.84 ms, TR = 2.2 s, flip angle: 8Ê.

Stimuli

We carefully selected 6 types of color-diagnostic objects of 3 color categories (Red: strawberry, watermelon; Green: cabbage, kiwi; Yellow: banana, corn) as stimuli, adhering to the following principles:

1. We chose fruits and vegetables of one diagnostic color based on the monkeys' prior experiences. For example, apples were excluded since monkeys in our facility have encountered and consumed red, green, and yellow varieties. Conversely, cabbage, despite the potential for different colors such as green and purple, was chosen for the green category, which was the only one provided to the animals in our facility.
2. All the monkeys used in these experiments had similar previous experiences with the selected fruits and vegetables. Monkeys have been exposed to the fruits and vegetables used in the present study for 5 to 6 years, with similar frequency each year, to ensure their nutritional needs and rich environments.

In addition, during the whole study, all monkeys were fed daily the 6 kinds of fruits and vegetables used in the experiments: strawberry, watermelon, cabbage, kiwi, banana, and corn.

Color images of the aforementioned fruits and vegetables were obtained from the internet. To minimize the potential confounding effects of low-level features on the following analyses, we carefully selected and preprocessed our stimuli. Firstly, we matched the size (the number of pixels, S6B Fig) of foreground stimuli. As for shape, we balanced the similarity of shapes for the red and green color-diagnostic categories by ensuring that the shape similarity within the same color category was not significantly different from the similarity between color categories (S6A Fig). However, aside from bananas and corn, identifying other fruits or vegetables with exclusively yellow color and which monkeys encounter as frequently as other objects used in the present study posed difficulties. Therefore, despite having a dissimilar shape in comparison to the objects in the other 2 color categories (S6A Fig), bananas and corn were still selected in the present study.

Shape similarity calculation. To quantify the shape dissimilarity between objects, we extracted the object shape boundaries for each image. Subsequently, we computed the Procrustes distance [71], which is a widely accepted method for calculating shape dissimilarity. This distance measure enables the translation, reflection, and orthogonal rotation of the shape matrix, facilitating the calculation of the minimum distance between 2 shapes by minimizing the effect of the presentation position and angle of the objects. Finally, we obtained the average shape similarity by averaging the shape similarity (1 minus the shape dissimilarity) across all pairs of images for each pair of objects.

Color similarity calculation. We also evaluated the real color similarity among the 6 types of objects. Specifically, we first extracted the average RGB values from the original color images. Subsequently, we calculated the color similarity between pairs of images by employing the Euclidean distance measurement, as described by Eq 1. Lastly, we computed the average color similarity by taking the mean across all pairs of images for each object pair.

$$\mathit{Color\ Similarity} = 1 - \frac{\overline{(R1 - R2)^2 + (G1 - G2)^2}}{}$$

Where R1, G1, and B1 represent the red, green, and blue values of Image 1, respectively. Similarly, R2, G2, and B2 represent the red, green, and blue values of Image 2, respectively.

Experimental design and

categories (i.e., green strawberry, green watermelon, red cabbage, and red kiwi) by swapping the colors [55]. As such, the overall colors and shapes of true-colored and false-colored categories were fully matched. In the fMRI experiment, there were 8 kinds of object blocks (2 color categories × 2 object categories × true-/false-color). The fMRI design of this experiment was the same as Exp 2. Each monkey was scanned in 2 to 4 sessions, resulting in a total of 20 to 24 runs used in the final analyses (M1: 20 runs, M2: 21 runs, M3: 24 runs).

To avoid interference between experiments caused by the potential learning effect, we conducted the experiments in the following order: Exp 2, Exp 1, and Exp 3. The behavioral experiment was conducted after all fMRI experiments.

fMRI data analysis

Functional data were preprocessed using Analysis of Functional NeuroImages software (AFNI) [75]. For each session, images were realigned to the volume with the minimum outlier. Then, the data were smoothed with a 2-mm full-width half-maximum Gaussian kernel. Signal intensity was normalized to the mean signal value within each run. We performed a single univariate linear model fit to estimate the response amplitude for each condition. The model included a hemodynamic response predictor for each category and regressors of no interest (baseline, movement parameters from realignment corrections, and signal drifts). A general linear model and an MION kernel were used to model the hemodynamic response function. All fMRI signals throughout the paper have been inverted so that an increase in signal intensity indicates an increase in activation. To identify the anatomical regions for defining ROIs in each monkey, we aligned statistical map images onto images of the symmetric NIMH Macaque Template (NMT) v2 [76]. Then, we projected our statistical results onto a rendered and inflated version of the NMT v2 cortical surface.

Definition of regions of interest (ROIs)

Color patches. First, to obtain the regions sensitive to colors, we compared chromatic grating conditions to the corresponding achromatic grating ones. To further equal the subjective luminance, in accordance with established research in monkeys [37,77], we identified specific chromatic grating conditions that elicited the weakest response in the area MT. Previous studies have demonstrated that responses to moving chromatic gratings in MT, which is specialized to process moving stimuli, can be employed to infer subjective equiluminance [78,79]: MT responds less strongly to moving chromatic gratings if the foreground and background within the chromatic gratings are equiluminant. As such, we identified the chromatic grating conditions that elicited the weakest response in MT, in which the more equiluminant chromatic gratings, the weaker responses evoked [77]. Then, the corresponding achromatic grating conditions were defined as the ones that yielded similar response magnitudes to the selected chromatic grating conditions in V1 [38]. In this way, any region that shows a greater response to equiluminant color than to achromatic luminance can therefore be interpreted as likely making a contribution to hue processing. We identified the color patches for each monkey using the contrast of the above-defined chromatic grating condition versus the corresponding achromatic grating condition (yellow grating versus 50% achromatic grating for M1 and M2; green grating versus 25% achromatic grating for M3). According to previous research [37] and the location of face patches in each monkey, we defined 7 color patches (see S1 Table for the correspondence between names of color patches in the present study and previous studies [37]) that were consistently presented in at least 1 hemisphere across all 3 monkeys at $p < 0.05$ (uncorrected): the color patch around V4d (V4d_c), V4v (V4v_c), TEO (TEO_c), TEpd (TEpd_c), TEad (TEad_c), TEav (TEav_c), and the border between area TEa and IPa (TEa_c)

[76,80,81]. Notedly, in 2 monkeys, several color patches in the right hemisphere (i.e., TEpd_c, TEav_c, and TEa_c in M1 and TEad_c in M2) showed relatively weak color bias as in the previous study [37]. We switched the achromatic grating to the next lower level (i.e., from 50% to 25%) to localize them ($p < 0.05$, uncorrected). We defined 3.5-mm radius spheres centered at each cluster mass. To perform the MVPA, the top 50 color-bias voxels within the spheres were selected to yield the final color patches. Given the lack of consistency and small sample size, we refrain from discussing further any left versus right hemispheric differences in the present manuscript, even slight variations were noted. The color patches from both hemispheres (100 voxels) were collapsed respectively in the following ROI analyses and MVPA.

To ensure greater consistency in the locations of the color patches across different monkeys, we conducted a group analysis across the 6 hemispheres from the 3 monkeys (see S2 Text and S12 Fig). Due to the limited number of monkey subjects, we considered each hemisphere as a sample for the group analysis. Despite inter-animal variability, the color patches identified at the individual level were found in close proximity to the color patches identified at the group level.

True-false ROIs. As previous studies have revealed the critical role of perirhinal circuits in the ATL in object-associative memory retrieval [26,42], we mainly looked into the 2 key nodes in this circuit: TP and PR. With the contrast of true- and false-colored objects, we observed consistent bilateral activated clusters in all 3 monkeys in TP but not in PR at $p < 0.05$ (uncorrected) (Figs 3A and S13A). In 2 of 3 monkeys, only unilateral activated clusters in PR could be found at $p < 0.05$ (uncorrected), while the contralateral PR clusters only showed at a lenient threshold (left PR in M1: $p < 0.20$, uncorrected; right PR in M2: $p < 0.25$, uncorrected). For the ROI analyses, to avoid the problem of double dipping [82], we split the data yielding 4 combinations and then conducted the ROI analyses [83,84] (S26 Fig). Specifically, we used half of the categories to define true-false voxels with the contrast of true- versus false-colored objects and then conducted the following ROI analyses on the other half of the categories (e.g., defining with true-colored cabbage and strawberry versus false-colored ones, then measuring responses on kiwi and watermelon). For each combination, the top 10 true-false voxels were selected within the anatomical mask of TP/PR from the D99 digital atlas [76,80] to yield each sub-ROI. All 4 combinations were analyzed and then averaged to produce the final results for each monkey. We also defined the ROI for the amygdala in the same way as above. For the MVPA, to ensure the location of ROIs for the univariate analysis and MVPA was close, we collapsed the 4 sub-ROIs and then generated a continuous combined mask, and then selected the top 50 true-false voxels. Note that, for PR, the same definition method as for TP could not yield 50 true-false voxels within PR. We conducted MVPA based on all survived voxels (33 to 35 voxels). To eliminate the impact of the number of voxels on MVPA, we also opted to directly select the top 50 true-false voxels from the anatomical mask of PR, yielding similar results (S27 Fig). To investigate the learning effect in the true- and false-colored objects viewing experiment, we divided the data from the middle into 2 halves (first and second half) for each monkey: M1: 2 versus 2 sessions (12 versus 8 runs); M2: 2 versus 2 sessions (11 versus 10 runs); M3 1 versus 1 session (11 versus 13 runs). Note that the analyses for the true- and false-colored object viewing experiment were conducted when the first and second halves were separated or combined.

Multivoxel pattern analysis (MVPA)

It is worth noting that the classification analysis is widely utilized in studies focusing on memory and imagination [11,40,55,85±87]. To facilitate meaningful comparisons between our study in monkeys and previous studies involving humans, we employed classification analysis. We applied LDA classifiers to analyze data based on CoSMoMVPA [88]. Prior to analyses, data were normalized using z-scoring to eliminate the impact of activation intensity to a certain extent [88]. During the chromatic and achromatic grating viewing experiment, we performed three-way classifications for chromatic gratings (i.e., Red, Green, and Yellow) and achromatic gratings (i.e., 25%, 50%, and 75% luminance contrast), respectively. A leave-one-out procedure was conducted. That is, for one iteration, N-1 runs were used for training, and the left-out run was used for testing. To test whether color patches were capable of differentiating between grayscale objects from different diagnostic color categories, we performed the classification of grayscale objects with different memory colors first. Eight-fold cross-validation analyses were conducted: training on half of the grayscale objects (e.g., strawberry, cabbage, and banana) on all runs and testing on the rest half of the grayscale objects (e.g., watermelon slice, kiwi slice, and corn) on each run, in the grayscale object viewing experiment. Accuracy rates from all 8 folds cross-validation analyses were averaged to yield the classification accuracy. To avoid the confounds of object shape, we further excluded objects with yellow diagnostic color (i.e., banana and corn) due to their relatively elongated shapes and did the classification again (4-fold cross-validation). To further verify the memory color representation of grayscale objects from different diagnostic color categories, predicting the color information of grayscale objects, three-way color classifiers (i.e., Red, Green, and Yellow) were trained on activity patterns elicited by the chromatic grating stimuli and then tested on responses to three grayscale object categories [10,40]. Note that all the runs in the chromatic and achromatic grating viewing experiment were used for training, and testing was conducted for each run in the grayscale object viewing experiment. These memory color decoding methods allowed us to examine the classifier's ability to discriminate based on (memory) color information alone, independent of shape. By employing these methods, we minimized the contribution of low-level features to the decoding results. In the true- and false-colored objects viewing experiment, two-way classifiers (i.e., true- and false-colored objects) were trained. Then, the same leave-one-out procedure as described above was conducted. When decoding object identity, all true-colored objects from the true- and false-colored object viewing experiment were used. Specifically, we trained a four-way classifier (red strawberry, red watermelon, green cabbage, green kiwi) and employed the leave-one-out procedure. Finally, for all MVPA, data from all iterations were averaged, yielding the final classification accuracy.

To investigate whether other brain areas beyond the functionally defined color patches and the true-false ROIs also code color knowledge, we performed whole-brain searchlight analyses (50 voxels for each sphere). Classification methods were the same as those used in the ROI-based decoding analyses.

Statistical analysis

All analyses were conducted using SPSS (v25) software (SPSS, Chicago, Illinois, USA), Matlab 2016a (MathWorks, Natick, Massachusetts, United States) and ªRº statistical programming language (R Foundation for Statistical Computing, R Development Core Team, 2017). We perform GLMMs to compare responses to chromatic and achromatic grating in color patches, with Monkey, Session, and Run as random factors [89,90]. Notably, to avoid the double-dipping problem, we performed the ROI analyses based on the responses to the gratings that were not used to define the color patches. When comparing the responses to 3 categories of grayscale objects in color patches and true-false ROIs, we also employed GLMM. Similarly, GLMMs were conducted to compare the responses to true- and false-colored objects in all the defined ROIs. To further explore the potential effects of learning, GLMMs were also conducted with Period (first half and second half of sessions) and True-False as fixed factors with Monkey, Session, and Run as random factors.

For the results of MVPA, to limit the possibility of result bias by a single monkey, we also performed GLMMs to compare decoding accuracy with the chance level, with Monkey, Session, and Run as random factors. Considering the binomial distribution nature of decoding accuracy [91,92], we employed a binomial target distribution with a log link function in the present study.

FDR corrections were conducted to adjust multiple ROIs ($n = 7$ for all the analyses for color patches, $n = 2$ for all the analyses for ATL) [33].

The binomial tests were conducted for the searchlight decoding analyses [85,93], in which accuracy was estimated on the total number of correctly classified samples given the overall number of cross-validation folds.

Supporting information

S1 Fig. Experimental procedures and results of the behavioral experiment. (A) The trial procedure: fixation, free viewing, and reward after successful trial completion. (B) From left to right, the proportion of fixation time averaged across 2 monkeys and for each monkey. (C) From left to right, the proportion of first fixation averaged across 2 monkeys and for each monkey. Bars display mean values +/− SEM. Red asterisks indicate a significant difference between responses evoked by true- and false-colored stimuli in B and C; $^{**}p < 0.01$, $^{***}p < 0.001$. The data underlying this figure are available in S1 Data.
(PDF)

S2 Fig. FMRI responses and decoding results in color patches in the chromatic and achromatic gratings viewing experiment. (A) Averaged fMRI responses elicited by chromatic and achromatic gratings, which were not used to define color patches, in color patches across all 3 subjects. (B) Chromatic and achromatic decoding accuracy when training the classifier to distinguish among the 3 chromatic/achromatic gratings in N-1 runs and testing on the left-out run. Black asterisks indicate a significant difference from the chance level (0.333 in B, indicated by the dash lines), and red ones indicate a significant difference between chromatic and achromatic gratings; $^{*}q < 0.05$, $^{**}q < 0.01$, $^{***}q < 0.001$. The data underlying this figure are available in S1 Data.
(PDF)

S3 Fig. Decoding results in color patches in the chromatic and achromatic gratings viewing experiment in each subject. Bars display mean values +/− SEM. Black asterisks indicate a significant difference from the chance level (0.333, indicated by the dash lines), and red ones indicate a significant difference between chromatic and achromatic gratings; $^{*}p < 0.05$, $^{**}p < 0.01$, $^{***}p < 0.001$. The numbers above the bars indicate p-values that are marginally significant ($p < 0.1$). The data underlying this figure are available in S1 Data.
(PDF)

S4 Fig. FMRI responses to 3 color-diagnostic grayscale objects. (A±C) Averaged fMRI responses to 3 categories of color-diagnostic grayscale objects in color patches defined on individual activation maps (A) and by the group analysis (B) and in ATL (C) across all 3 monkeys. Bars display mean values +/− SEM. The data underlying this figure are available in S1 Data.
(PDF)

S5 Fig. Classification of grayscale objects with different memory colors in color patches excluding shape confound. (A) The results of classification of grayscale objects with 3 different memory colors: training the classifier to distinguish among the half of grayscale objects (e.g., strawberry, cabbage, and banana) and testing on the other half (e.g., watermelon slice,

kiwi slice, and corn). Successful decoding was found in V4d_c, V4v_c, TEO_c, TEad_c, and TEa_c. (B) The ªmemoryº color and shape similarities between training and test objects with red and green memory colors in various fold combinations. The second rows exhibited non-simultaneous alterations in ªmemoryº color and shape similarity matrix values (framed by the red square), which were used to compute decoding accuracy rates in (C). For example, in Fold 1, we trained the classifier to distinguish the grayscale images of cabbage and watermelon and tested on kiwi and strawberry. In this case, kiwi might be correctly classified along with cabbage based on either color or shape, as for both properties, kiwi is more similar to cabbage than to watermelon. By contrast, strawberry is closer to watermelon in color but to cabbage in shape. Therefore, if a classifier identifies strawberries as more similar to watermelons with an accuracy significantly higher than chance, such a classifier could not be based on shape. (C) The results of the classification of grayscale objects with red and green memory colors in color patches based on the second rows of folds. Successful decoding was found in V4d_c, TEO_c, and TEad_c after excluding shape confound. Bars display mean values +/− SEM. Black asterisks indicate a significant difference from the chance level (0.333 in A, 0.5 in C, indicated by the dashed lines); *$q < 0.05$, **$q < 0.01$, ***$q < 0.001$. The data underlying this figure are available in S1 Data.
(PDF)

S6 Fig. Statistical information of low-level stimulus features. (A) The averaged shape similarity matrix of grayscale images from different color categories. (B) Pixel counts of foreground of grayscale images from different color categories. Bars display mean values +/− SEM. (C) Luminance histograms of foreground of grayscale images from different color categories. The data underlying this figure are available in S1 Data.
(PDF)

S7 Fig. Classification of grayscale objects with red and green memory colors in each subject. (A±C) Classification of grayscale objects with red and green memory colors in each monkey. Bars display mean values +/− SEM. Black asterisks indicate a significant difference from the chance level (0.5, indicated by the dashed lines); *$p < 0.05$, **$p < 0.01$, ***$p < 0.001$. (D±F) The results of whole-brain searchlight analyses for decoding memory color in each subject shown on the template inflated surface. White solid lines indicate color patches and TP defined for each subject. The data underlying this figure are available in S1 Data.
(PDF)

S8 Fig. Memory color decoding and searchlight results based on chromatic gratings training in each subject. (A±C) Memory color decoding accuracy in color patches in each monkey. Bars display mean values +/− SEM. Black asterisks indicate a significant difference from the chance level (0.333, indicated by the dashed lines); *$p < 0.05$, **$p < 0.01$, ***$p < 0.001$. The numbers above the bars indicate p-values that are marginally significant ($p < 0.1$). (D±F) The results of whole-brain searchlight analyses for decoding memory color in each subject shown on the template inflated surface. White solid lines indicate color patches and TP defined for each subject. The data underlying this figure are available in S1 Data.
(PDF)

S9 Fig. Results of memory color decoding in V1. (A) Results of classification of grayscale objects with red and green memory colors: training the classifier to distinguish half set of the red and green color-diagnostic grayscale objects and testing on the other half in Exp 2. (B) Results of memory color decoding based on chromatic gratings training: training the classifier to distinguish among 3 chromatic gratings in Exp 1 and then testing on 3 categories of grayscale objects in Exp 2. Bars display mean values +/− SEM. Black asterisks indicate a significant

difference from the chance level (0.5 in A, 0.333 in B, indicated by the dashed lines); *$p < 0.05$. The data underlying this figure are available in S1 Data.
(PDF)

S10 Fig. Averaged fMRI responses to true- and false-colored objects in color patches across 3 monkeys. No significant differences were found between responses evoked by true- and false-color objects. Bars display mean values +/– SEM. The data underlying this figure are available in S1 Data.
(PDF)

S11 Fig. True-False color decoding and searchlight results in each subject. (A±C) True-False color decoding accuracy in color patches in each monkey. Bars display mean values +/– SEM. Black asterisks indicate a significant difference from the chance level (0.5, indicated by the dashed lines); *$p < 0.05$, **$p < 0.01$, ***$p < 0.001$. (D±F) The results of whole-brain searchlight analyses for decoding true-false color for each subject shown on the template inflated surface. White solid lines indicate color patches and TP defined for each subject. The data underlying this figure are available in S1 Data.
(PDF)

S12 Fig. Results of color patches defined by the group analysis. (A) Color biased clusters defined by the group analysis based on the 6 hemispheres from the 3 subjects ($p < 0.01$, uncorrected) from Exp 1 are shown on the lateral view of the template inflated surface of the left hemisphere. Red solid lines indicate that clusters could be defined at $p < 0.05$ (uncorrected), while white solid lines indicate clusters that could be defined when adjusting the contrasted achromatic grating to the next lower level (i.e., from 50% to 25% in M1 and M2, $p < 0.01$, uncorrected) to account for the

in the coronal slices for each of the 3 subjects (M1 to M3) at $p < 0.05$, respectively. Each slice's anterior/posterior position is indicated on the top left corner (mm relative to the interaural canal). (D) Averaged fMRI responses to true- and false-colored objects in PR across all 3 subjects based on all the sessions [$F_{(1,128)} = 0.050$, q = 0.823, $\eta 2 < 0.001$; two-tailed]. (E) Averaged fMRI responses to true- and false-colored objects in PR across all 3 subjects from the first and second halves of sessions [the interaction effect between Period (first half versus second half) and True-False across 3 monkeys: $F_{(1,126)} = 0.305$, q = 0.582, $\eta 2 = 0.002$]. The data underlying this figure are available in S1 Data.
(PDF)

S14 Fig. Regions exhibiting stronger responses to false-colored stimuli compared to true-colored stimuli. Results of the whole-brain analysis at the group level are shown on the lateral view of the template inflated surface.
(PDF)

S15 Fig. The interaction effect in TP for each subject. (A) The conjunction map that combined the true-color versus false-color contrast with the interaction effect between Period (first half versus second half of sessions) and True-False for each of the 3 subjects (M1 to M3) at $p < 0.01$. Each slice's anterior/posterior position is indicated on the top left corner (mm relative to the interaural canal). (B±D) FMRI responses to true- and false-colored objects in TP from the first and second halves of sessions for each subject, respectively. Individual analyses demonstrated similar trends for the 3 monkeys, although the results were not significant, likely due to the limited sample size used as a result of the request to avoid double dipping and the impact of the learning effect. (E±G) fMRI responses to true- and false-colored objects in TP for each session in each subject. Bars display mean values +/– SEM. Red asterisks indicate a significant difference between responses evoked by true- and false-colored stimuli; *$p < 0.05$, **$p < 0.01$, ***$p < 0.001$. The data underlying this figure are available in S1 Data.
(PDF)

S16 Fig. TP exhibiting the interaction effect at the group level. (A) Averaged fMRI responses to true- and false-colored objects in TP across all sessions and subjects. To avoid the possible circularity, we used a one-half set of the true- and false-colored objects to define the true-false ROI in TP and then examined the true-false differentiation effect on the other half set of the stimuli. Due to this strict approach, differences between true- and false-colored objects when combining all sessions were not visible [$F_{(1,128)} = 0.274$, q = 0.823, $\eta 2 = 0.002$; two-tailed]. (B) Averaged fMRI responses to true- and false-colored objects in TP across all 3 subjects from the first and second halves of sessions. We did observe an interesting learning effect: a significant interaction effect between Period and True-False across 3 monkeys [$F_{(1,126)} = 11.006$, q = 0.002, $\eta 2 = 0.080$; two-tailed]. To further investigate this interaction effect, we conducted post hoc analyses. In the first half of the sessions, the ROI analysis revealed that TP responded significantly more strongly to true-colored objects across 3 monkeys [$t_{(126)} = 3.420$, q = 0.002, Cohen's d = 0.609; two-tailed]. The differences in averaged responses evoked by true- and false-colored objects across all 3 monkeys observed in the first half of the sessions vanished in the second half. Bars display mean values +/– SEM. Red asterisks indicate a significant difference between responses evoked by true- and false-colored stimuli; **$q < 0.01$. (C) Regions exhibiting the interaction effect between Period (first half versus second half of sessions) and True-False of the whole-brain analysis at the group level are shown on the lateral view of the template inflated surface. White solid lines indicate the location of TP from the D99 atlas [76,80]. The data underlying this figure are available in S1 Data.
(PDF)

S17 Fig. FMRI responses to true- and false-colored objects in PR from the first and second halves of sessions for each subject. (A±C) FMRI responses to true- and false-colored objects in PR from the first and second halves of sessions for each subject, respectively. Bars display mean values +/– SEM. Red asterisks indicate a significant difference between responses evoked by true- and false-colored stimuli; **$p < 0.01$. The numbers above the bars indicate p-values that are marginally significant ($p < 0.1$). The data underlying this figure are available in S1 Data.
(PDF)

S18 Fig. True-false color decoding accuracy in true-false ROIs for each subject. (A±C) True-False color decoding accuracies in TP and PR in each monkey when combining all sessions, respectively. (D, E) True-false color decoding accuracies in TP and PR in each monkey based on the first and second halves of sessions, respectively. Bars display mean values +/– SEM. Black asterisks indicate a significant difference from the chance level (0.5, indicated by the dashed lines); *$p < 0.05$, **$p < 0.01$. The numbers above the bars indicate p-values that are marginally significant ($p < 0.1$). The data underlying this figure are available in S1 Data.
(PDF)

S19 Fig. Averaged true-false color decoding accuracy in true-false ROIs across 3 monkeys. (A) True-False color decoding accuracies in TP and PR across 3 monkeys based on the first and second halves of sessions. (B) True-False color decoding accuracies across 3 monkeys when combining all sessions. Bars display mean values +/– SEM. Black asterisks indicate a significant difference from the chance level (0.5, indicated by the dashed lines); *$q < 0.05$. The data underlying this figure are available in S1 Data.
(PDF)

S20 Fig. Averaged fMRI responses and true-false color decoding in color patches based on the first and second halves of sessions. (A) Averaged fMRI responses to true- and false-colored objects in color patches across all three subjects for the first and second halves of sessions. (B) True-false color decoding accuracies across 3 monkeys for the first and second halves of sessions. Bars display mean values +/– SEM. Black asterisks indicate a significant difference from the chance level (0.5, indicated by the dashed lines); *$q < 0.05$. The data underlying this figure are available in S1 Data.
(PDF)

S21 Fig. True-false color decoding accuracies in each monkey for the first and second halves of sessions. Bars display mean values +/– SEM. Black asterisks indicate a significant difference from the chance level (0.5, indicated by the dashed lines). Red asterisks indicate a significant difference between the first and second half of sessions; *$p < 0.05$. The numbers above the bars indicate p-values that are marginally significant ($p < 0.1$). The data underlying this figure are available in S1 Data.
(PDF)

S22 Fig. Memory color decoding results in true-false ROIs for each monkey. (A) Results of classification of grayscale objects with red and green memory colors in each monkey: training the classifier to distinguish half set of the red and green color-diagnostic grayscale objects and testing on the other half in Exp 2. (B) Results of memory color decoding based on chromatic gratings training in each monkey: training the classifier to distinguish among three chromatic gratings in Exp 1 and then testing on 3 categories of grayscale objects in Exp 2. Bars display mean values +/– SEM. Dashed lines indicate the chance level (0.5 in A and 0.333 in B); *$p < 0.05$. The numbers above the bars indicate p-values that are marginally significant

($p < 0.1$). The data underlying this figure are available in S1 Data.
(PDF)

S23 Fig. Averaged fMRI responses to true- and false-colored objects in the amygdala across all 3 subjects from the first and second halves of sessions. The main effect of true-false [$F_{(1,126)} = 2.348$, $p = 0.128$] and the interaction effect between Period and true-false [$F_{(1,126)} = 0.733$, $p = 0.393$] were not significant. Bars display mean values +/– SEM. n.s., not significant. The data underlying this figure are available in S1 Data.
(PDF)

S24 Fig. Results of object identity encoding in TP and PR. (A) Object identity encoding in TP and PR across 3 monkeys utilizing all true-colored objects in Exp 3. The group analysis yielded a trend but not significant decoding accuracy above the chance level for TP [$F_{(1,128)} = 2.281$, $p = 0.067$, q = 0.126, one-tailed]. (B±D) Object identity encoding in TP and PR in each monkey, respectively. Bars display mean values +/– SEM. Dashed lines indicate the chance level (0.25). The numbers above the bars indicate p-values that are marginally significant ($p < 0.1$). The data underlying this figure are available in S1 Data.
(PDF)

S25 Fig. Color selectivity in color patches. (A) Color selectivity in color patches defined by the individual analysis. (B) Correlations between the color selectivity and decoding accuracies of classification of grayscale objects with red and green =underl(twod].

values +/– SEM. Dashed lines indicate the chance level (0.5 in A and C; 0.333 in B; 0.25 in D); *$q < 0.05$. The data underlying this figure are available in S1 Data.
(PDF)

S1 Table. The correspondence between names of color patches in the present study and previous studies [37].
(DOCX)

S2 Table. GLMM results of main effects of true-false in color patches.
(DOCX)

S3 Table. GLMM results of fMRI responses to true- and false-colored objects in TP and PR for each subject.
(DOCX)

S4 Table. GLMM results of interaction effects between Period and true-false across 3 monkeys in color patches.
(DOCX)

S5 Table. Parameters of chromatic and achromatic stimuli used in Exp 1.
(DOCX)

S1 Text. Experimental procedures and data analysis for behavioral experiment.
(DOCX)

S2 Text. Definition of color patches by the group analysis and the corresponding results.
(DOCX)

S3 Text. Calculation of color selectivity index.
(DOCX)

S1 Data. Data underlying the plots in all figures.
(XLSX)

Acknowledgments

We thank Tianshu Yang and Zhaojin Cheng for the animal surgery.

Author Contributions

Conceptualization: Minghui Zhao, Xiaoying Wang, Yanchao Bi, Ning Liu.

Data curation: Minghui Zhao, Ning Liu.

Formal analysis: Minghui Zhao, Ning Liu.

Funding acquisition: Xiaoying Wang, Yanchao Bi, Ning Liu.

Investigation: Minghui Zhao, Yumeng Xin, Haoyun Deng, Zhentao Zuo, Ning Liu.

Methodology: Minghui Zhao, Yumeng Xin, Xiaoying Wang, Yanchao Bi, Ning Liu.

Project administration: Xiaoying Wang, Yanchao Bi, Ning Liu.

Resources: Zhentao Zuo, Ning Liu.

Software: Minghui Zhao, Yumeng Xin, Ning Liu.

Supervision: Xiaoying Wang, Yanchao Bi, Ning Liu.

Validation: Minghui Zhao, Ning Liu.

Visualization: Minghui Zhao.

Writing ± original draft: Minghui Zhao, Xiaoying Wang, Yanchao Bi.

Writing ± review & editing: Minghui Zhao, Yumeng Xin, Haoyun Deng, Zhentao Zuo, Xiaoying Wang, Yanchao Bi, Ning Liu.

References

1. Miller G. How are memories stored and retrieved? Science. 2005; 309(5731):92. https://doi.org/10.1126/science.309.5731.92 PMID: 15994538
2. Binder JR, Desai RH. The neurobiology of semantic memory. Trends Cogn Sci. 2011; 15(11):527±536. https://doi.org/10.1016/j.tics.2011.10.001 PMID: 22001867
3. Binder JR, Desai RH, Graves WW, Conant LL. Where Is the Semantic System? A Critical Review and Meta-Analysis of 120 Functional Neuroimaging Studies. Cereb Cortex. 2009; 19(12):2767±2796.
4. Martin A. GRAPES-Grounding representations in action, perception, and emotion systems: How object properties and categories are represented in the human brain. Psychon Bull Rev. 2016; 23(4):979±990. https://doi.org/10.3758/s13423-015-0842-3 PMID: 25968087
5. Mahon BZ, Caramazza A. A critical look at the embodied cognition hypothesis and a new proposal for grounding conceptual content. J Physiol Paris. 2008; 102(1±3):59±70. https://doi.org/10.1016/j.jphysparis.2008.03.004 PMID: 18448316
6. Bi Y. Dual coding of knowledge in the human brain. Trends Cogn Sci. 2021; 25(10):883±895. https://doi.org/10.1016/j.tics.2021.07.006 PMID: 34509366
7. Ralph MA, Jefferies E, Patterson K, Rogers TT. The neural and computational bases of semantic cognition. Nat Rev Neurosci. 2017; 18(1):42±55. https://doi.org/10.1038/nrn.2016.150 PMID: 27881854
8. Simmons WK, Ramjee V, Beauchamp MS, McRae K, Martin A, Barsalou LW. A common neural substrate for perceiving and knowing about color. Neuropsychologia. 2007; 45(12):2802±2810. https://doi.org/10.1016/j.neuropsychologia.2007.05.002 PMID: 17575989
9. Wang X, Han Z, He Y, Caramazza A, Song L, Bi Y. Where color rests: spontaneous brain activity of bilateral fusiform and lingual regions predicts object color knowledge performance. Neuroimage. 2013; 76:252±263. https://doi.org/10.1016/j.neuroimage.2013.03.010 PMID: 23518009
10. Bannert Michael M, Bartels A. Decoding the Yellow of a Gray Banana. Curr Biol. 2013; 23(22):2268±2272. https://doi.org/10.1016/j.cub.2013.09.016 PMID: 24184103
11. Bannert MM, Bartels A. Human V4 Activity Patterns Predict Behavioral Performance in Imagery of Object Color. J Neurosci. 2018; 38(15):3657±3668. https://doi.org/10.1523/JNEUROSCI.2307-17.2018 PMID: 29519852
12. Fernandino L, Binder JR, Desai RH, Pendl SL, Humphries CJ, Gross WL, et al. Concept Representation Reflects Multimodal Abstraction: A Framework for Embodied Semantics. Cereb Cortex. 2016; 26(5):2018±2034. https://doi.org/10.1093/cercor/bhv020 PMID: 25750259
13. Miceli G, Fouch E, Capasso R, Shelton JR, Tomaiuolo F, Caramazza A. The dissociation of color from form and function knowledge. Nat Neurosci. 2001; 4(6):662±667. https://doi.org/10.1038/88497 PMID: 11369950
14. Stasenko A, Garcea FE, Dombovy M, Mahon BZ. When concepts lose their color: a case of object-color knowledge impairment. Cortex. 2014; 58:217±238. https://doi.org/10.1016/j.cortex.2014.05.013 PMID: 25058612
15. Martin A, Haxby JV, Lalonde FM, Wiggs CL, Ungerleider LG. Discrete Cortical Regions Associated with Knowledge of Color and Knowledge of Action. Science. 1995; 270(5233):102±105. https://doi.org/10.1126/science.270.5233.102 PMID: 7569934
16. Clarke A, Tyler LK. Understanding What We See: How We Derive Meaning From Vision. Trends Cogn Sci. 2015; 19(11):677±687. https://doi.org/10.1016/j.tics.2015.08.008 PMID: 26440124
17. Fang Y, Wang X, Zhong S, Song L, Han Z, Gong G, et al. Semantic representation in the white matter pathway. PLoS Biol. 2018; 16(4):e2003993. https://doi.org/10.1371/journal.pbio.2003993 PMID: 29624578
18. Martin CB, Douglas D, Newsome RN, Man LL, Barense MD. Integrative and distinctive coding of visual and conceptual object features in the ventral visual stream. Elife. 2018:7.
19. Quian QR. Concept cells: the building blocks of declarative memory functions. Nat Rev Neurosci. 2012; 13(8):587±597. https://doi.org/10.1038/nrn3251 PMID: 22760181

20. Coutanche MN, Thompson-Schill SL. Creating Concepts from Converging Features in Human Cortex. Cereb Cortex. 2015; 25(9):2584±2593. https://doi.org/10.1093/cercor/bhu057 PMID: 24692512
21. Lambon Ralph MA, Sage K, Jones RW, Mayberry EJ. Coherent concepts are computed in the anterior temporal lobes. Proc Natl Acad Sci U S A. 2010; 107(6):2717±2722. https://doi.org/10.1073/pnas.0907307107 PMID: 20133780
22. Kim JS, Elli GV, Bedny M. Knowledge of animal appearance among sighted and blind adults. Proc Natl Acad Sci U S A. 2019; 116(23):11213±11222. https://doi.org/10.1073/pnas.1900952116 PMID: 31113884
23. Lupyan G. The Centrality of Language in Human Cognition. Language Learning. 2016; 66(3):516±553.
24. Lupyan G, Abdel Rahman R, Boroditsky L, Clark A. Effects of Language on Visual Perception. Trends Cogn Sci. 2020; 24(11):930±944. https://doi.org/10.1016/j.tics.2020.08.005 PMID: 33012687
25. Spelke ES. Core Knowledge, Language, and Number. Language Learning and Development. 2017; 13 (2):147±170.
26. Miyashita Y. Perirhinal circuits for memory processing. Nat Rev Neurosci. 2019; 20(10):577±592. https://doi.org/10.1038/s41583-019-0213-6 PMID: 31485007
27. Miyashita Y. Neuronal correlate of visual associative long-term memory in the primate temporal cortex. Nature. 1988; 335(6193):817±820. https://doi.org/10.1038/335817a0 PMID: 3185711
28. Sakai K, Miyashita Y. Neural organization for the long-term memory of paired associates. Nature. 1991; 354(6349):152±155. https://doi.org/10.1038/354152a0 PMID: 1944594
29. Naya Y, Yoshida M, Miyashita Y. Forward Processing of Long-Term Associative Memory in Monkey Inferotemporal Cortex. J Neurosci. 2003; 23(7):2861. https://doi.org/10.1523/JNEUROSCI.23-07-02861.2003 PMID: 12684473
30. Miyashita Y, Kameyama M, Hasegawa I, Fukushima T. Consolidation of Visual Associative Long-Term Memory in the Temporal Cortex of Primates. Neurobiol Learn Mem. 1998; 70(1):197±211. https://doi.org/10.1006/nlme.1998.3848 PMID: 9753597
31. Sakai K, Higuchi S-I, Miyashita Y. Single neurons in primate temporal cortex code both pictures of paired associates stored in long-term memory. Neurosci Res Suppl. 1991; 16:IX.
32. Naya Y, Yoshida M, Takeda M, Fujimichi R, Miyashita Y. Delay-period activities in two subdivisions of monkey inferotemporal cortex during pair association memory task. Eur J Neurosci. 2003; 18 (10):2915±2918. https://doi.org/10.1111/j.1460-9568.2003.03020.x PMID: 14656343
33. Landi SM, Freiwald WA. Two areas for familiar face recognition in the primate brain. Science. 2017; 357 (6351):591±595. https://doi.org/10.1126/science.aan1139 PMID: 28798130
34. Landi SM, Viswanathan P, Serene S, Freiwald WA. A fast link between face perception and memory in the temporal pole. Science. 2021; 373(6554):581±585. https://doi.org/10.1126/science.abi6671 PMID: 34210891
35. Vanduffel W, Zhu Q, Orban GA. Monkey cortex through fMRI glasses. Neuron. 2014; 83(3):533±550. https://doi.org/10.1016/j.neuron.2014.07.015 PMID: 25102559
36. Chang L, Bao P, Tsao DY. The representation of colored objects in macaque color patches. Nat Commun. 2017; 8(1):2064. https://doi.org/10.1038/s41467-017-01912-7 PMID: 29234028
37. Lafer-Sousa R, Conway BR. Parallel, multi-stage processing of colors, faces and shapes in macaque inferior temporal cortex. Nat Neurosci. 2013; 16(12):1870±1878. https://doi.org/10.1038/nn.3555 PMID: 24141314
38. Lafer-Sousa R, Conway BR, Kanwisher NG. Color-Biased Regions of the Ventral Visual Pathway Lie between Face- and Place-Selective Regions in Humans, as in Macaques. J Neurosci. 2016; 36 (5):1682±1697. https://doi.org/10.1523/JNEUROSCI.3164-15.2016 PMID: 26843649
39. Cox DD, Savoy RL. Functional magnetic resonance imaging (fMRI) ªbrain readingº: detecting and classifying distributed patterns of fMRI activity in human visual cortex. Neuroimage. 2003; 19(2):261±270. https://doi.org/10.1016/s1053-8119(03)00049-1 PMID: 12814577
40. Teichmann L, Grootswagers T, Carlson TA, Rich AN. Seeing versus knowing: The temporal dynamics of real and implied colour processing in the human brain. Neuroimage. 2019; 200:373±381. https://doi.org/10.1016/j.neuroimage.2019.06.062 PMID: 31254648
41. Vandenbroucke ARE, Fahrenfort JJ, Meuwese JDI, Scholte HS, Lamme VAF. Prior Knowledge about Objects Determines Neural Color Representation in Human Visual Cortex. Cereb Cortex. 2016; 26 (4):1401±1408. https://doi.org/10.1093/cercor/bhu224 PMID: 25323417
42. Nakamura K, Kubota K. The primate temporal pole: its putative role in object recognition and memory. Behav Brain Res. 1996; 77(1±2):53±77. https://doi.org/10.1016/0166-4328(95)00227-8 PMID: 8762159

43. Zeki S, Marini L. Three cortical stages of colour processing in the human brain. Brain. 1998; 121(Pt 9):1669±1685. https://doi.org/10.1093/brain/121.9.1669 PMID: 9762956

44. Bastin C, Besson G, Simon J, Delhaye E, Geurten M, Willems S, et al. An integrative memory model of recollection and familiarity to understand memory deficits. Behav Brain Sci. 2019; 42:e281. https://doi.org/10.1017/S0140525X19000621 PMID: 30719958

45. Holscher C, Rolls ET, Xiang J. Perirhinal cortex neuronal activity related to long-term familiarity memory in the macaque. Eur J Neurosci. 2003; 18(7):2037±2046. https://doi.org/10.1046/j.1460-9568.2003.02903.x PMID: 14622237

46. Ranganath C, Ritchey M. Two cortical systems for memory-guided behaviour. Nat Rev Neurosci. 2012; 13(10):713±726. https://doi.org/10.1038/nrn3338 PMID: 22992647

47. Sugiura M, Kawashima R, Nakamura K, Sato N, Nakamura A, Kato T, et al. Activation reduction in anterior temporal cortices during repeated recognition of faces of personal acquaintances. Neuroimage. 2001; 13(5):877±890. https://doi.org/10.1006/nimg.2001.0747 PMID: 11304083

48. Tomeo OB, Ungerleider LG, Liu N. Preference for Averageness in Faces Does Not Generalize to Non-Human Primates. Front Behav Neurosci. 2017; 11:129. https://doi.org/10.3389/fnbeh.2017.00129 PMID: 28744207

49. Taubert J, Wardle SG, Flessert M, Leopold DA, Ungerleider LG. Face Pareidolia in the Rhesus Monkey. Curr Biol. 2017; 27(16):2505±9 e2. https://doi.org/10.1016/j.cub.2017.06.075 PMID: 28803877

50. Taubert J, Flessert M, Wardle SG, Basile BM, Murphy AP, Murray EA, et al. Amygdala lesions eliminate viewing preferences for faces in rhesus monkeys. Proc Natl Acad Sci U S A. 2018; 115(31):8043±8048. https://doi.org/10.1073/pnas.1807245115 PMID: 30012600

51. Krassanakis V, Filippakopoulou V, Nakos B. EyeMMV toolbox: An eye movement post-analysis tool based on a two-step spatial dispersion threshold for fixation identification. Journal of Eye Movement. Research. 2014; 7(1).

52. Duyck M, Chang ALY, Gruen TJ, Tello LY, Eastman S, Fuller-Deets J, et al. Color Tuning of Face-Selective Neurons in Macaque Inferior Temporal Cortex. eNeuro. 2021; 8(2). https://doi.org/10.1523/ENEURO.0395-20.2020 PMID: 33483324

53. Dreksler N, Spence C. A Critical Analysis of Colour±Shape Correspondences: Examining the Replicability of Colour±Shape Associations. Perception. 2019; 10(2). https://doi.org/10.1177/2041669519834042 PMID: 30956786

54. Zelazny A, Liu X, Sørensen TA. Shape±color associations in an unrestricted color choice paradigm. Front Psychol. 2023:14.

55. Teichmann L, Quek GL, Robinson AK, Grootswagers T, Carlson TA, Rich AN. The Influence of Object-Color Knowledge on Emerging Object Representations in the Brain. J Neurosci. 2020; 40(35):6779±6789. https://doi.org/10.1523/JNEUROSCI.0158-20.2020 PMID: 32703903

56. Naya Y, Yoshida M, Miyashita Y. Backward Spreading of Memory-Retrieval Signal in the Primate Temporal Cortex. Science. 2001; 291(5504):661±664. https://doi.org/10.1126/science.291.5504.661 PMID: 11158679

57. Takeda M, Koyano KW, Hirabayashi T, Adachi Y, Miyashita Y. Top-Down Regulation of Laminar Circuit via Inter-Area Signal for Successful Object Memory Recall in Monkey Temporal Cortex. Neuron. 2015; 86(3):840±852. https://doi.org/10.1016/j.neuron.2015.03.047 PMID: 25913857

58. Chabardès S, Kahane P, Minotti L, Hoffmann D, Benabid A-L. Anatomy of the temporal pole region. Epileptic Disord. 2002; 4(S1):S9±S15. PMID: 12424085

59. Herzog AG, Van Hoesen GW. Temporal neocortical afferent connections to the amygdala in the rhesus monkey. Brain Res. 1976; 115(1):57±69. https://doi.org/10.1016/0006-8993(76)90822-2 PMID: 824015

60. Wang X, Men W, Gao J, Caramazza A, Bi Y. Two Forms of Knowledge Representations in the Human Brain. Neuron. 2020; 107(2):383±93 e5. https://doi.org/10.1016/j.neuron.2020.04.010 PMID: 32386524

61. Bottini R, Ferraro S, Nigri A, Cuccarini V, Bruzzone MG, Collignon O. Brain Regions Involved in Conceptual Retrieval in Sighted and Blind People. J Cogn Neurosci. 2020; 32(6):1009±1025. https://doi.org/10.1162/jocn_a_01538 PMID: 32013684

62. Quian QR. No Pattern Separation in the Human Hippocampus. Trends Cogn Sci. 2020; 24(12):994±1007. https://doi.org/10.1016/j.tics.2020.09.012 PMID: 33162337

63. Santos LR, Hauser MD, Spelke ES. Recognition and categorization of biologically significant objects by rhesus monkeys (Macaca mulatta): the domain of food. Cognition. 2001; 82(2):127±155. https://doi.org/10.1016/s0010-0277(01)00149-4 PMID: 11716832

64. Striem-Amit E, Wang X, Bi Y, Caramazza A. Neural representation of visual concepts in people born blind. Nat Commun. 2018; 9(1):5250. https://doi.org/10.1038/s41467-018-07574-3 PMID: 30531889

65. Bernardi S, Salzman CD. The contribution of nonhuman primate research to the understanding of emotion and cognition and its clinical relevance. Proc Natl Acad Sci U S A. 2019; 116(52):26305±26312. https://doi.org/10.1073/pnas.1902293116 PMID: 31871162

66. Hansen T, Pracejus L, Gegenfurtner KR. Color perception in the intermediate periphery of the visual field. J Vis. 2009; 9(4):26:1±12. https://doi.org/10.1167/9.4.26 PMID: 19757935

67. Tootell RB, Silverman MS, Hamilton SL, De Valois RL, Switkes E. Functional anatomy of macaque striate cortex. III Color J Neurosci. 1988; 8(5):1569±1593.

68. Liu N, Kriegeskorte N, Mur M, Hadj-Bouziane F, Luh WM, Tootell RB, et al. Intrinsic structure of visual exemplar and category representations in macaque brain. J Neurosci. 2013; 33(28):11346±11360. https://doi.org/10.1523/JNEUROSCI.4180-12.2013 PMID: 23843508

69. Liu N, Hadj-Bouziane F, Jones KB, Turchi JN, Averbeck BB, Ungerleider LG. Oxytocin modulates fMRI responses to facial expression in macaques. Proc Natl Acad Sci U S A. 2015; 112(24):E3123±E3130. https://doi.org/10.1073/pnas.1508097112 PMID: 26015576

70. Leite FP, Tsao D, Vanduffel W, Fize D, Sasaki Y, Wald LL, et al. Repeated fMRI using iron oxide contrast agent in awake, behaving macaques at 3 Tesla. Neuroimage. 2002; 16(2):283±294. https://doi.org/10.1006/nimg.2002.1110 PMID: 12030817

71. Goodall C. Procrustes Methods in the Statistical Analysis of Shape. 1991; 53(2):285±321.

72. Kleiner M, Brainard DH, Pelli D, Ingling A, Murray R, Broussard C. What's new in Psychtoolbox-3. Perception. 2007; 36:1±16.

73. Wu Y, Zhao M, Deng H, Wang T, Xin Y, Dai W, et al. The neural origin for asymmetric coding of surface color in the primate visual cortex. Nat Commun. 2024; 15(1). https://doi.org/10.1038/s41467-024-44809-y PMID: 38225259

74. Edwards R, Xiao D, Keysers C, FoÈldiaÂk P, Perrett D. Color sensitivity of cells responsive to complex stimuli in the temporal cortex. J Neurophysiol. 2003; 90(2):1245±1256. https://doi.org/10.1152/jn.00524.2002 PMID: 12904507

75. Cox RW. AFNI: Software for Analysis and Visualization of Functional Magnetic Resonance Neuroimages. Comput Biomed Res. 1996; 29(3):162±173. https://doi.org/10.1006/cbmr.1996.0014 PMID: 8812068

76. Jung B, Taylor PA, Seidlitz J, Sponheim C, Perkins P, Ungerleider LG, et al. A comprehensive macaque fMRI pipeline and hierarchical atlas. Neuroimage. 2021; 235:117997. https://doi.org/10.1016/j.neuroimage.2021.117997 PMID: 33789138

77. Conway BR, Tsao DY. Color architecture in alert macaque cortex revealed by FMRI. Cereb Cortex. 2006; 16(11):1604±1613. https://doi.org/10.1093/cercor/bhj099 PMID: 16400160

78. Dobkins KR, Thiele A, Albright TD. Comparison of red-green equiluminance points in humans and macaques: evidence for different L:M cone ratios between species. J Opt Soc Am A Opt Image Sci Vis. 2000; 17(3):545±56. https://doi.org/10.1364/josaa.17.000545 PMID: 10708036

79. Dobkins KR, Albright TD. Behavioral and neural effects of chromatic isoluminance in the primate visual motion system. Vis Neurosci. 1995; 12(2):321±332. https://doi.org/10.1017/s0952523800008002 PMID: 7786853

80. Saleem KS, Avram AV, Glen D, Yen CC, Ye FQ, Komlosh M, et al. High-resolution mapping and digital atlas of subcortical regions in the macaque monkey based on matched MAP-MRI and histology. Neuroimage. 2021; 245:118759. https://doi.org/10.1016/j.neuroimage.2021.118759 PMID: 34838750

81. Seidlitz J, Sponheim C, Glen D, Ye FQ, Saleem KS, Leopold DA, et al. A population MRI brain template and analysis tools for the macaque. Neuroimage. 2018; 170:121±131. https://doi.org/10.1016/j.neuroimage.2017.04.063 PMID: 28461058

82. Kriegeskorte N, Simmons WK, Bellgowan PS, Baker CI. Circular analysis in systems neuroscience: the dangers of double dipping. Nat Neurosci. 2009; 12(5):535±540. https://doi.org/10.1038/nn.2303 PMID: 19396166

83. Gomez J, Barnett MA, Natu V, Mezer A, Palomero-Gallagher N, Weiner KS, et al. Microstructural proliferation in human cortex is coupled with the development of face processing. Science. 2017; 355(6320):68±71. https://doi.org/10.1126/science.aag0311 PMID: 28059764

84. Jiahui G, Yang H, Duchaine B. Developmental prosopagnosics have widespread selectivity reductions across category-selective visual cortex. Proc Natl Acad Sci U S A. 2018; 115(28):E6418±E6427. https://doi.org/10.1073/pnas.1802246115 PMID: 29941554

85. Dubois J, de Berker AO, Tsao DY. Single-unit recordings in the macaque face patch system reveal limitations of fMRI MVPA. J Neurosci. 2015; 35(6):2791±2802. https://doi.org/10.1523/JNEUROSCI.4037-14.2015 PMID: 25673866

86. Li S, Zeng X, Shao Z, Yu Q. Neural Representations in Visual and Parietal Cortex Differentiate between Imagined, Perceived, and Illusory Experiences. J Neurosci. 2023; 43(38):6508±6524. https://doi.org/10.1523/JNEUROSCI.0592-23.2023 PMID: 37582626

87. Taubert J, Japee S, Patterson A, Wild H, Goyal S, Yu D, et al. A broadly tuned network for affective body language in the macaque brain. Sci Adv. 2022; 8(47):eadd6865. https://doi.org/10.1126/sciadv.add6865 PMID: 36427322

88. Oosterhof NN, Connolly AC, Haxby JV. CoSMoMVPA: Multi-Modal Multivariate Pattern Analysis of Neuroimaging Data in Matlab/GNU Octave. Front Neuroinform. 2016; 10:27. https://doi.org/10.3389/fninf.2016.00027 PMID: 27499741

89. Liu N, Behrmann M, Turchi JN, Avidan G, Hadj-Bouziane F, Ungerleider LG. Bidirectional and parallel relationships in macaque face circuit revealed by fMRI and causal pharmacological inactivation. Nat Commun. 2022; 13(1):6787.

90. Garcia-Pelegrin E, Miller R, Wilkins C, Clayton NS. Manual action expectation and biomechanical ability in three species of New World monkey. Curr Biol. 2023; 33(9):1803±8 e2. https://doi.org/10.1016/j.cub.2023.03.023 PMID: 37019106

91. Setogawa T, Eldridge MAG, Fomani GP, Saunders RC, Richmond BJ. Contributions of the Monkey Inferior Temporal Areas TE and TEO to Visual Categorization. Cereb Cortex. 2021; 31(11):4891±4900. https://doi.org/10.1093/cercor/bhab129 PMID: 33987672

92. Pereira F, Mitchell T, Botvinick M. Machine learning classifiers and fMRI: A tutorial overview. Neuroimage. 2009; 45(1):S199±S209. https://doi.org/10.1016/j.neuroimage.2008.11.007 PMID: 19070668

93. Stelzer J, Chen Y, Turner R. Statistical inference and multiple testing correction in classification-based multi-voxel pattern analysis (MVPA): random permutations and cluster size control. Neuroimage. 2013; 65:69±82. https://doi.org/10.1016/j.neuroimage.2012.09.063 PMID: 23041526

94. Janssens T, Zhu Q, Popivanov ID, Vanduffel W. Probabilistic and single-subject retinotopic maps reveal the topographic organization of face patches in the macaque cortex. J Neurosci. 2014; 34(31):10156±10167. https://doi.org/10.1523/JNEUROSCI.2914-13.2013 PMID: 25080579